the First European Display Research Conference," Munich, p. 111, VDE-Verlag GmbH, Berlin (1981).
15. M. Gazard, "Handbook of Conducting Polymers," Vol. 1, T. J. Skotheim, Editor, p. 673, Marcel Dekker, Inc., New York (1986).
16. R. A. Bull, F. F. Fan, and A. J. Bard, *This Journal*, **129**, 1009 (1982).
17. P. Burgmayer and R. W. Murray, "Handbook of Conducting Polymers," Vol. 1, T. J. Skotheim, Editor, p. 507, Marcel Dekker, Inc., New York (1986).
18. G. B. Street, T. C. Clarke, M. Krounbi, K. K. Kanazawa, V. Lee, P. Pfluger, J. C. Scott, and G. Weiler, *Mos. Cryst. Liq. Cryst.*, **83**, 253 (1982).
19. S. Asavapiriyanont, G. K. Chandler, G. A. Gunawardena, and D. Pletcher, *J. Electroanal. Chem.*, **177**, 229 (1984).
20. T. Yeu, T. V. Nguyen, and R. E. White, *This Journal*, **135**, 1971 (1988).
21. T. Yeu and R. E. White, *ibid.*, **137**, 1327 (1990).
22. W. G. Cochran, *Proc. Cambridge Phil. Soc.*, **30**, 365 (1934).
23. M. H. Rogers and G. N. Lance, *J. Fluid Mech.*, **7**, 617 (1960).
24. F. Fan and A. J. Bard, *This Journal*, **133**, 301 (1986).
25. S. Panero, P. Prosperi, S. Passerini, B. Scrosati, and D. D. Perlmutter, *ibid.*, **136**, 3729 (1989).
26. J. Tanguy, N. Mermilliod, and M. Hoclet, *ibid.*, **134**, 795 (1987).
27. N. Mermilliod, J. Tanguy, and F. Petiot, *ibid.*, **133**, 1073 (1986).
28. P. E. Gill, W. Murray, and M. H. Wright, "Practical Optimization," Academic Press, Inc., New York (1984).

Hydrous Oxide Film Growth on Amorphous Ni-Co Alloys

K. K. Lian*,[1] and V. I. Birss**

Chemistry Department, University of Calgary, Calgary, Alberta, T2N 1N4, Canada

ABSTRACT

The electrochemical behavior of a $Ni_{51}Co_{23}Cr_{10}Mo_7Fe_{5.5}B_{3.5}$ (weight percent) amorphous alloy ribbon has been investigated in alkaline solutions. When the metal is initially subjected to anodic potentials, an enriched Cr (and possibly B) surface layer is dissolved. Following this, a hydrous oxide film can be readily formed on the electrode surface by a continuous potential cycling method, to a thickness of up to *ca.* one micron. The film, which has an electrochemical signature which is very similar to the Ni(II)/Ni(III) transition, is electrochromic in nature and displays interference colors when still thin. The maximum growth rate of the film per cycle of potential has been found to be 0.15 to 0.20 mC/cm^2, achieved by optimization of the magnitude and time spent at the upper and lower potential limits.

There has been a significant amount of interest in the electrochemical behavior of glassy alloys since the earliest reports of their superior corrosion resistance and interesting mechanical, electrical, and magnetic properties (1-10). The low corrosion susceptibility of these materials is not unexpected, due to the virtual absence of classical grain boundaries and other crystalline defects, as well as the frequent presence of elements such as Cr, Ti, Nb, etc. (7, 11-20), which are known to promote the formation of protective oxide films in most environments. There have also been numerous reports concerning the electrocatalytic nature of particular amorphous alloys toward reactions such as hydrogen and oxygen evolution (21-27) and the hydrogenation of carbon monoxide (28, 29). This is also reasonable, as surface defect sites are known to play an important role in heterogeneous electrocatalytic reactions.

In the present study, an investigation of the electrochemical oxidation of an amorphous alloy, containing primarily Ni [51 weight percent (w/o)] and Co (23 w/o), was undertaken. Alkaline solutions were utilized in order to minimize the dissolution of these metals, and oxide growth behavior was compared with that observed at polycrystalline Ni and Co electrodes. Polycrystalline Ni electrodes have been studied extensively in the past in alkaline solutions (30-39), due to their important application in secondary batteries, in which the principal reaction involves the Ni(II)/(III) transition at *ca.* 1.4 V *vs.* RHE. Numerous investigations have indicated that Ni oxide films are hydrous in nature, and that they can be thickened by a particular continuous potential cycling regime (35-37). However, the resulting oxide and its growth behavior exhibit only some of the characteristics which are typical of other hydrous oxides, such as those formed at Ir (40-44), Rh (45), W (46), etc.

* Electrochemical Society Student Member.
** Electrochemical Society Active Member.
[1] Department of Metallurgy & Materials Science, University of Toronto, Toronto, Ontario, M5S 1A4, Canada.

At a fresh polycrystalline Co electrode, several different oxidation/reduction steps can be seen in the first sweep of a CV experiment (47-49). With continued potential cycling, the buildup of a hydrous oxide film occurs readily (47, 48, 50, 51), similar to the case at numerous other metals (40-46), where it is believed that new oxide film is formed during each excursion to positive potentials, while negative potentials are required in order to release the newly formed oxide from the metal surface to the overlying hydrous oxide film (40, 41). The principal electrochemical reaction [Co(III)/(IV)] occurs in the range of 1.0 to 1.5 V *vs.* RHE. Oxidized Co electrodes, as well as Co/Ni oxide electrodes, have also been investigated (52-54) with respect to the kinetics of the oxygen evolution reaction (OER) at these materials.

The purpose of this research was to determine how the presence of both Co and Ni, as well as several secondary elements (Cr, Mo, and B) influence the nature of oxide growth and the properties of the resulting oxide film. Also, it was of interest to examine the impact of the amorphous structure of the substrate on the properties of the electrochemically formed oxide films. Both electrochemical and *ex situ* surface analytical techniques were employed in this work in an attempt to answer these questions.

Experimental

Cyclic voltammetry was carried out with the use of a Hokuto-Denko HA301 potentiostat and a Tacussel GSATP function generator, or with the EG&G PARC 175/173 combination when infrared compensation was required. Either a HP 7045B X/Y recorder or a Nicolet 3091 digital oscilloscope were employed to record the electrochemical data. The working electrode (WE) used in all of these experiments was a melt-spun $Ni_{51}Co_{23}Cr_{10}Mo_7Fe_{5.5}B_{3.5}$ (composition given in terms of w/o) glassy alloy, provided by Allied-Signal Corporation in the form of a ribbon 25 mm wide

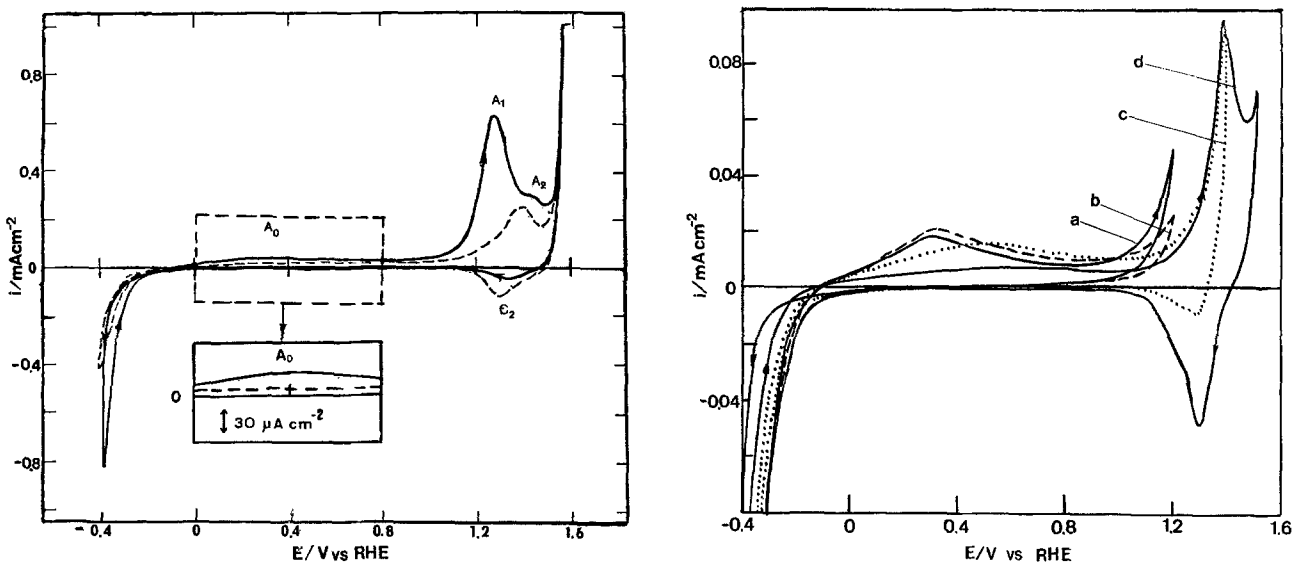

Fig. 1. (Left) The first (——) and second (---) cycles of potential of 'as-received' Ni-Co alloy in 1M NaOH; s = 100 mV/s. (Right) Sequential CVs of 'as-received' alloy to various E_+ values in 1M NaOH; s = 10 mV/s.

and 10 μm thick, from which small pieces were cut to serve as electrodes. Although the two sides of the ribbon appeared differently visually, they were shown in this work to be very similar electrochemically, and therefore, both sides were studied at once. A second ribbon-cast amorphous ribbon ($Co_{63}Cr_{27}Ni_3Fe_3W_4$, Allied-Signal) was also briefly investigated, primarily to establish the influence of Cr on the electrochemistry of the Ni/Co amorphous alloy.

Before each experiment, the WE was rinsed with distilled water, ultrasonically cleaned in acetone, and then press-contacted to a silver wire in a Teflon holder. Solution was prevented from reaching the Ag wire by the firm application of either Teflon tape or parafilm, or the use of epoxy glue. The apparent geometric area, typically *ca.* 0.1 cm^2, was used as the electrode surface area for oxidized electrodes. The ribbon was too fragile to be polished mechanically, either before or after an experiment. However, it could be re-used by removing the oxide film by dipping in 3*M* H_2SO_4. The reference electrode (RE) used in this work was a reversible hydrogen electrode, while the counterelectrode (CE) was a large area Pt gauze. All chemicals used in this work were A.C.S. grade and all water was triply distilled. Solutions were deaerated by bubbling high-purity argon through or above the cell solution at all times. All experiments were carried out at room temperature.

A Cambridge S-150 scanning electron microscope (SEM) was employed to determine the structure and composition of oxide films formed electrochemically at the WE surface. Auger electron spectroscopy (AES) and x-ray photoelectron spectroscopy (XPS), with Ar ion sputtering capabilities (PHI 548 XPS/AES and PHI 600 SAM at CANMET, Department of Energy, Mines and Resources, Ottawa, Ontario and a VG ESCA III, Alcan International Limited, Kingston, Ontario) were also used in this work. An I.L. VIDEO 11 AA/AE spectrophotometer was employed in the analysis of cell solutions for the presence of dissolved metals.

Results and Discussion

Electrochemical behavior of 'as-received' Ni-Co amorphous alloy.—A typical cyclic voltammogram (CV) observed in the first cycle of potential (——) in the range between the hydrogen (HER) and oxygen evolution reactions is shown in Fig. 1a. A small anodic peak (A_0) can be seen at *ca.* 0.30 V; it is most similar in potential and shape to the Ni/Ni(OH)$_2$ peak seen at Ni electrodes (Fig. 2a). The potential of the Co/Co(OH)$_2$ process at Co electrodes is somewhat more negative than this (Fig. 2b). At *ca.* 1.25-1.3 V, a much larger peak (A_1) is seen in Fig. 1a, followed by a smaller one (A_2) at *ca.* 1.45 V. Only a single, relatively small cathodic peak (C_2) is observed at *ca.* 1.35 V in the first reverse scan. By comparison with Fig. 2, it could be suggested that peak A_1 reflects some component of Co oxidation, and A_2 the Ni(II) to Ni(III) conversion process, with only Ni(III) reduction (peak C_2) being observed in the cathodic sweep. It is of interest that if the first sweep is preceded by extensive hydrogen evolution, then the A_0 peak and the electrochemical response up to peak A_1 is enhanced and appears to be very similar to that at a fresh Ni electrode, while peaks A_1, A_2, and C_2 are unaffected by this pretreatment.

In the second cycle of potential (Fig. 1, left ---), peak A_0 is diminished in size (typical for both Ni and Co electrodes), the rate of the HER is substantially decreased, and peak A_1 has now completely disappeared. Peaks A_2 and C_2 now have an appearance more similar to the Ni(II)/(III) peaks (cf. Fig. 2, upper left), and little evidence for Co oxide electrochemistry is present. With continued cycling, peaks A_2/C_2 increase in size (Fig. 3); this will be discussed in greater detail later in this paper.

Figure 1, right, indicates that if the potential of a fresh glassy alloy electrode is not extended positively beyond 1.2 V, the current in the region of the foot of A_1 decreases with each cycle of potential, consistent with the result of Fig. 1, left, and indicating that the process in A_1 becomes deactivated with time or that it involves the complete consumption of a reactant. A subsequent complete cycle of potential reveals only peaks A_2/C_2 and diminished rates of both the HER and peak A_0, as in Fig. 1, left.

It is instructive to compare the charge densities observed in Fig. 1a with those seen in the first few cycles of potential at polycrystalline Ni and Co electrodes. Peak A_1 typically involves *ca.* 3 mC/cm^2, while the A_2/C_2 peaks involve *ca.* 0.2 mC/cm^2, which is in the range of one monolayer of film material. In contrast, the Ni(II)/(III) peaks at polycrystalline Ni electrodes can involve a charge density of *ca.* 5 mC/cm^2. Co electrodes appear to form only a few monolayers of oxide in the first scan of potential. Therefore, peaks A_2/C_2 appear to have features which are not precisely those of either Ni or Co. Rather a new set of characteristics, reminiscent of both Co and Ni, is observed.

In a previous study of a $NiCo_2O_4$ spinel electrode (52) and another of a polycrystalline $NiCo_2$ alloy (53), similar peaks to A_1 have been noted. In the former case, no explanation was provided for its presence and no indication was given as to its fate with time of cycling. The A_1-like peak was reported to be seen only at rapid sweep rates, contrary to the present work, in which A_1 is seen over a wide range of sweep rates (*ca.* 10 to 400 mV/s) (55). In the study of Haenen *et al.* (53), the first sweep of potential of a fresh $NiCo_2$ alloy clearly reveals the superimposed characteristics of both Co and Ni. The A_1-like peak, which is much broader than that in Fig. 1a, appears very similar to that seen in this potential range of the Co CV (Fig. 2, upper right). With con-

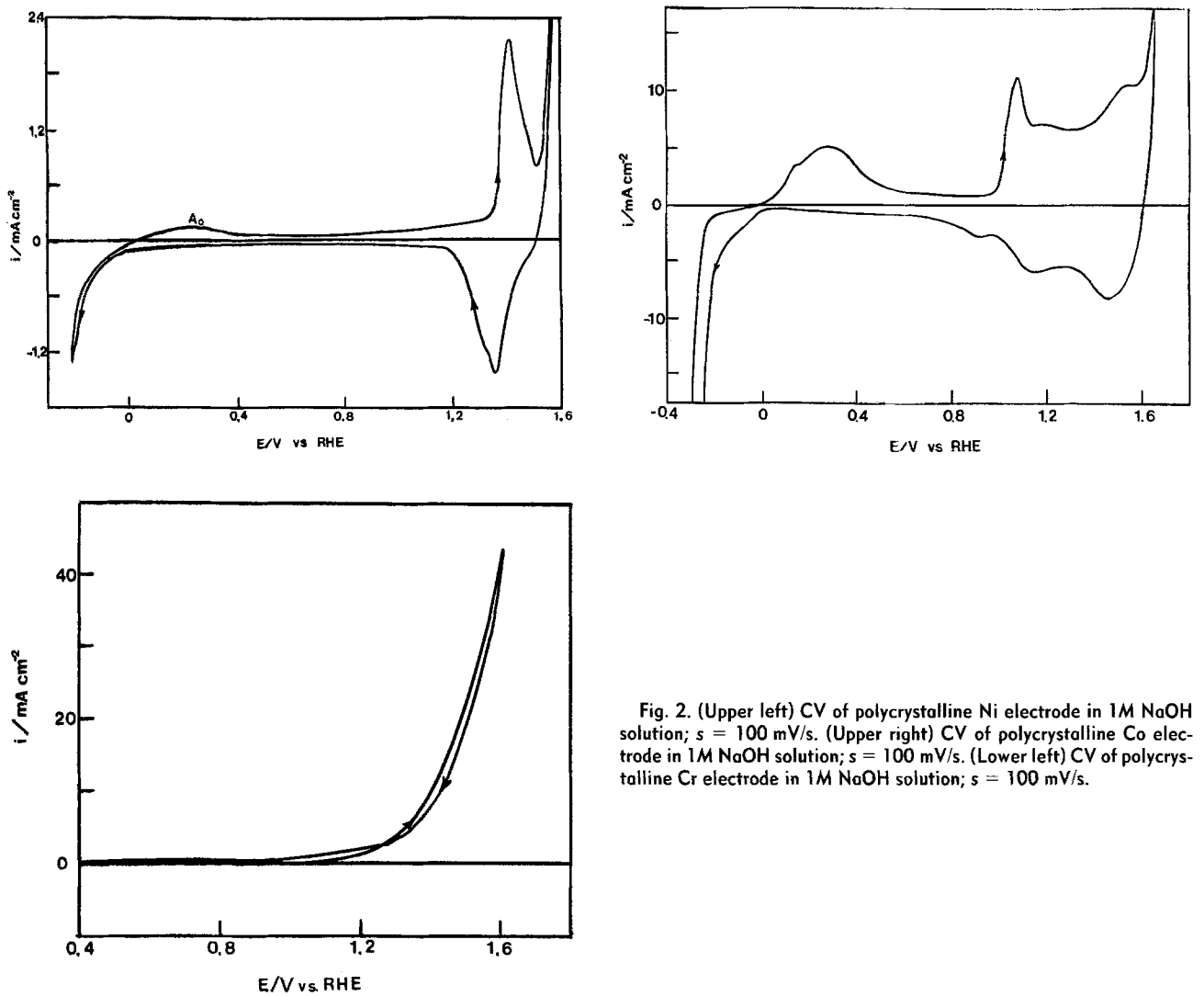

Fig. 2. (Upper left) CV of polycrystalline Ni electrode in 1M NaOH solution; s = 100 mV/s. (Upper right) CV of polycrystalline Co electrode in 1M NaOH solution; s = 100 mV/s. (Lower left) CV of polycrystalline Cr electrode in 1M NaOH solution; s = 100 mV/s.

tinuous cycling, however, the Co features disappear (53), and the CV response closely resembles that of Ni, despite the 2:1 ratio of Co:Ni. Therefore, although there are some general similarities in the appearance of the A_1-like region in these two previous papers, there also appear to be distinct and important differences, as compared to the present work.

One interpretation of the A_1 peak, which would be specific to the particular amorphous alloy under study here, is that it reflects the dissolution of a component of the alloy surface. Indeed, comparison of Fig. 1, right, with the CV for Cr in alkaline solutions (Fig. 2, lower left) supports the notion that Cr is selectively stripped from the alloy surface during the first sweep of potential. This supposition has been tested in the following way. A series of six identical 'as-received' alloy samples were subjected to potential sweeps over the A_1 peak in a small volume of solution, which was then analyzed by atomic absorption spectroscopy (AAS). By comparison with a Cr standard solution, produced by controlled anodic polarization of a polycrystalline Cr electrode, the results show conclusively that Cr is dissolving in the range of potential of the A_1 peak. Another argument in support of the dissolution of Cr in peak A_1 is found from the results of the electrochemical oxidation of the Co-Cr amorphous alloy. The Cr concentration obtained from the AA analysis of the solution in which this alloy was oxidized was found to be 7.5 times higher than that for the Ni-Co alloy, consistent with the higher Cr content of the Co-Cr alloy. It should be noted that both Mo and B are also susceptible to dissolution under these conditions. However, the relatively low concentration of these elements in the alloy made their analysis difficult.

The fact that A_1 is substantially larger than the other peaks in the first scan of potential (Fig. 1a) implies that Cr is enriched at the alloy surface in the 'as-received' state. This would be consistent with the reported tendency of Cr to concentrate in the surface region of glassy alloys (7, 11-15). In support of this, Fig. 4 shows the AES depth profile of the "as-received" alloy (depths are estimated from sputter time/depth data for Al_2O_3). Cr does appear to be enriched in the surface region, along with oxygen (Fig. 4), to an apparent depth of *ca.* 100 Å.

It is of interest that the charge density in peak A_1 of *ca.* 3 mC/cm^2, which could therefore be presumed to reflect the oxidation of Cr(III) oxide to a soluble Cr(VI) form, would be consistent with the dissolution of *ca.* 5 monolayers of a purely Cr surface. As the concentration of Cr (Fig. 4) is in the range of 20-30%, and as some Mo and B dissolution is also likely to be occurring in A_1, this charge density probably represents dissolution from a surface region in the range of 10 equivalent monolayers. Figure 4 shows that Co is depleted from the surface region of the "as-received" alloy. This argues against the interpretation of A_1 as being related to Co oxidation and instead, is consistent with the conspicuous absence of Co electrochemistry (cf. Fig. 1, left, with 2, upper right) in all subsequent scans and the fact that no trace of dissolved Co was found by AA analysis of the solutions.

The XPS data shows that Ni is almost completely in the metallic state at the "as-received" alloy surface, which is rather unusual for this element. Interestingly, a recent XPS study of thin CoNi films has also shown that after exposure to oxygen, Co is oxidized, while Ni remains in the metallic state (56). In the present work, Co, Mo, and Fe, although at low levels at the surface of the amorphous alloy, are also found to be in the metallic state. Cr is found to be *ca.* 80% in the form of either CrOOH or Cr_2O_3, while boron is also found to be *ca.* 95% oxidized. This indicates that Cr, and possibly B, may have served as oxygen getters at the

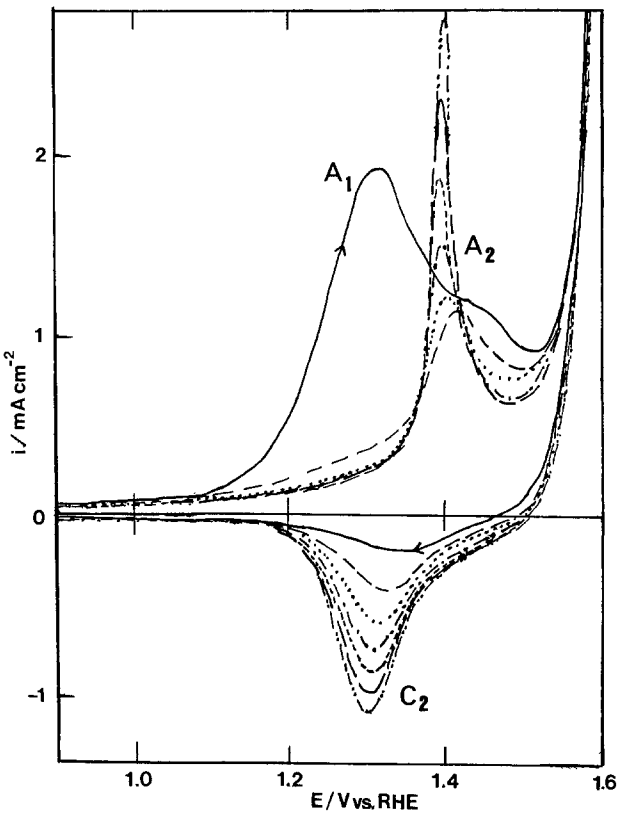

Fig. 3. Electrochemical response of 'as-received' Ni-Co alloy in 1M NaOH, with continuous potential cycling (cycles no. 1 to 7) from −0.2 to 1.6 V; s = 100 mV/s.

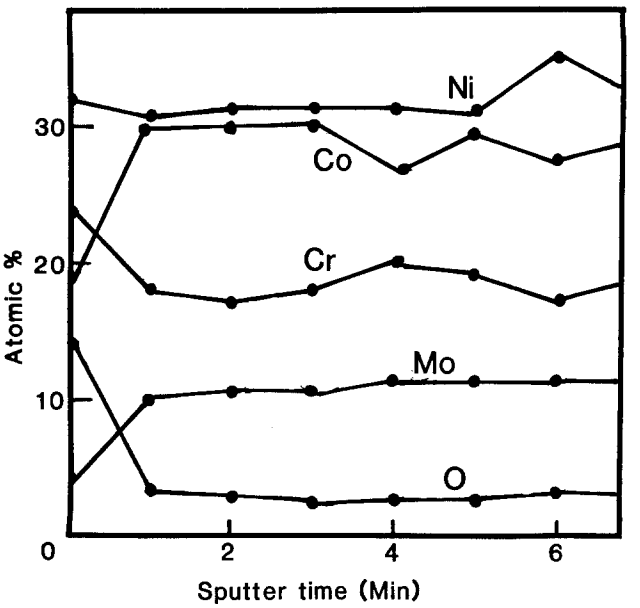

Fig. 4. AES depth profile of 'as-received' Ni-Co alloy.

alloy surface, and confirms earlier suggestions (7, 11-18) that the surface of Cr-containing amorphous alloys is essentially in the Cr oxide form, consistent with the excellent corrosion resistance of these alloys. It is worthy of note that the loss of the enriched Cr oxide surface layer after anodic polarization in alkaline solutions would leave the alloy in a more corrosion-susceptible form in acid solutions. Also, it appears that surface changes induced by potential cycling in basic solutions result in a significant change in the electrocatalysis of the HER (Fig. 1, left).

Electrochemical oxidation of amorphous Co-Ni alloy.— Figure 3 clearly shows that peak A_2 becomes narrower (peak width at half-height, $w_{1/2}$ = 30-40 mV) and moves negatively (from 1.43 to 1.38 V) in the first few cycles of potential, while C_2 also shifts by *ca.* 50 mV, but remains relatively broad ($w_{1/2}$ = 85-90 mV). In comparison, $w_{1/2}$ is *ca.* 95-100 mV and *ca.* 125 mV for the anodic and cathodic Ni(II)/(III) peaks, respectively, at polycrystalline Ni electrodes (Fig. 2, upper left). It has been suggested (32, 36, 37) that the broadness of the peaks of Ni reflects the presence of two closely spaced pairs of peaks, possibly related to the oxidation/reduction of two different phases of Ni oxide. If this is the case, the relative narrowness of the peaks shown in Fig. 3 may indicate that only one Ni oxide phase is stable when the oxide is formed at an amorphous substrate.

Although the anodic charge densities are difficult to calculate due to the overlap of A_2 with the OER, the anodic and cathodic charges in A_2 and C_2 in Fig. 3 were found to be very similar. The distinct difference in the first and subsequent scans over A_2/C_2 is indicative of a marked change in the nature of the electrode surface. If Cr (and Mo and B) are removed from the electrode surface in the first few scans, it is likely that the electrochemical response of the Ni and Co sites would reflect this change. Therefore, the increase in size and the negative shift of the A_2/C_2 peaks may indicate that Ni-Co atoms were initially accessible only on a small portion of the original alloy surface, and that only a dilute, laterally noninteractive, thin Ni-Co oxide film could be formed. After the loss of the secondary elements, and possibly some surface rearrangement, it is reasonable to suggest that a Ni-Co oxide film could more completely cover the electrode surface. Under these conditions, a characteristic potential, similar to that of the Ni(II)/(III) process, is now observed. As stated above, there is no clear electrochemical signature observed for the presence of Co in these films.

With continuous potential cycling, peaks A_2/C_2 increase steadily in size (Fig. 3), while the current negative of the peaks remains constant, and even decreases somewhat in the range of the HER. This is very reminiscent of the thickening of a hydrous oxide film at metals such as Co (47) and Ir (40), but is different from the behavior at Ni (35, 36, 55), where all of the currents increase slowly with cycling between extreme potentials, although the A_2/C_2 peaks increase at a somewhat higher rate than the others.

As the hydrous oxide film thickens at the Ni-Co electrode, the electrode surface exhibits electrochromism, being darker at potentials positive of A_2 and lighter at negative potentials. Furthermore, with increasing magnitude of the A_2/C_2 peaks, the color of the electrode surface changed from yellowish, to light brown, purple, blue, and then yellowish/green again, typical of the development of interference colors with changing film thickness. This is not observed with Ni or Ir electrodes under the same experimental conditions, and may reflect a higher degree of smoothness of the amorphous alloy surface, or a greater homogeneity of this oxide film *vs.* those formed at polycrystalline electrodes.

As a measure of the extent of oxide film growth, a similar approach was utilized here as in the electrochemical formation of Ru and Ir hydrous oxide films in previous work (57). This was based on establishing the ratio of the charge density observed in the A_2/C_2 peaks at the end of the growth period to that at the start of the experiment, leading to the determination of a charge enhancement factor (CEF) (57). Because of the overlap of peaks A_1 and A_2 and the uncertainty in the true magnitude of C_2 [due to some simultaneous metal (*e.g.*, Cr) dissolution] in the first cycle of potential (Fig. 1), the charge density in the A_2/C_2 peaks in the second cycle was examined for its reproducibility and appropriateness in defining an initial surface condition. This was found to be in the range of *ca.* 0.2 to 0.35 mC/cm^2, the variation probably reflecting a somewhat different roughness factor from sample to sample, not unexpected after the dissolution of part of the metal surface in the prior sweep. As will be shown later in this paper, there is strong evidence that the oxidation/reduction of one monolayer of oxide (in peaks A_2/C_2) on these amorphous Ni-Co alloy electrodes involves *ca.* 0.15 mC/cm^2, indicating an electrode roughness factor of up to *ca.* 2.3 after secondary metal dissolution. In the determination of the CEF for

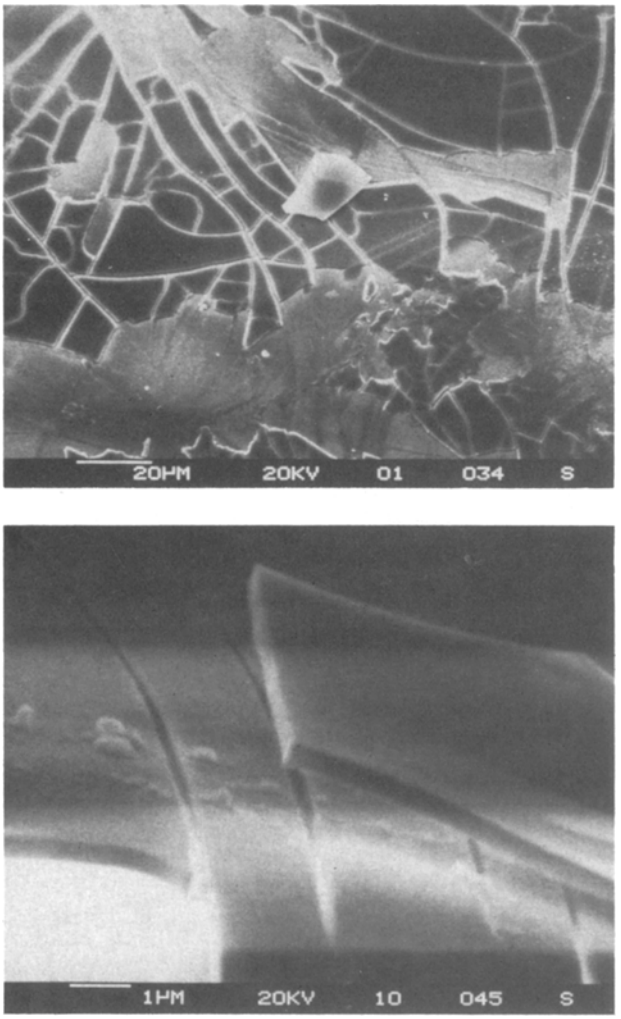

Fig. 5. SEM photographs of oxidized Ni-Co amorphous alloy. (Upper) CEF = 250, (lower) CEF = 400.

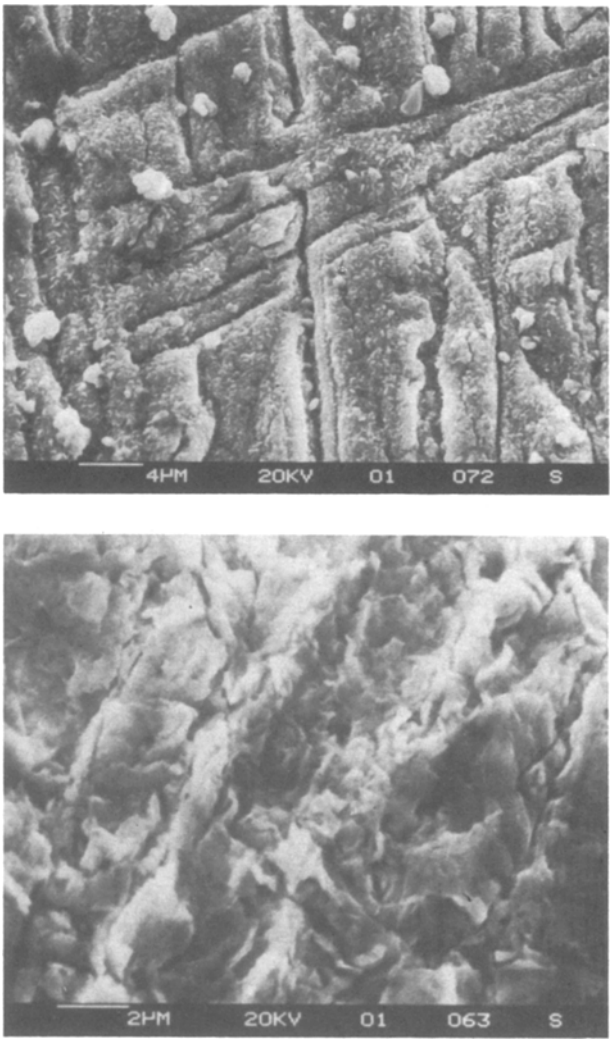

Fig. 6. (Upper) SEM photograph of oxide film formed electrochemically at polycrystalline Co electrode. (Lower) SEM photograph of electrochemically oxidized polycrystalline Ni electrode.

each oxide film grown in this work, the value of 0.15 mC/cm^2 was used as the charge density of the first monolayer of oxide film. Oxide films having a CEF of *ca.* 100 were routinely obtained, while CEFs of up to 500 could be reached after more than 24 h of potential cycling.

One of the characteristic features of hydrous oxide films is their morphology, as seen by SEM. Figure 5 shows that a typical mud-cracked microstructure is seen when electrochemically oxidized amorphous Ni/Co alloys are exposed to the high vacuum conditions of the SEM chamber. The oxide film appears virtually identical to those formed at Ir (44, 57) and Pt (58, 59), and similar to those formed at Co electrodes (Fig. 6, top). In contrast, the oxide formed at Ni electrodes by extensive potential cycling to the potentials required to grow a hydrous oxide film, *i.e.*, −0.5 to 1.55 V, appears to be much rougher, and a mud-cracked structure is not discernible (Fig. 6, bottom). This points out another dissimilarity between oxide growth at Ni and these amorphous Ni/Co alloys.

As has been the case for other hydrous oxide films which have been studied, *e.g.*, Ir (44, 57), Pt (58, 59), Rh, and Co (60), it is possible to establish the (dry) thickness of these oxides by SEM at the regions where oxide fragments have broken away from the underlying substrate (Fig. 5, bottom) and correlate these with the CEF. Figure 7 shows such a plot for CEFs determined at 100 mV/s. In the case of the thickest oxide, not all of the film was oxidized/reduced in the sweep, *i.e.*, the reaction was now diffusion-controlled (61) and the true CEF is higher than shown.

The CEF value can be considered to represent the number of equivalent monolayers of oxide present. From the linear portion of the plot in Fig. 7, it would appear that one monolayer of oxide has a thickness of *ca.* 9 Å. This is similar to the thickness of one monolayer of hydrous Ir oxide, found to be *ca.* 10 Å per monolayer of oxide film (41).

One of the very puzzling aspects of the CV response of oxidized Co-Ni alloy electrodes (Fig. 3), also referred to above, is the absence of any electrochemical features which can be related directly to Co oxidation/reduction (cf. Fig. 2, upper right). In fact, the behavior is most similar to that of Ni oxide electrodes (Fig. 2, upper left). An AES depth profile of an oxide film which had been oxidized to a CEF of *ca.* 100 (Fig. 8) clearly demonstrates that Co is fully

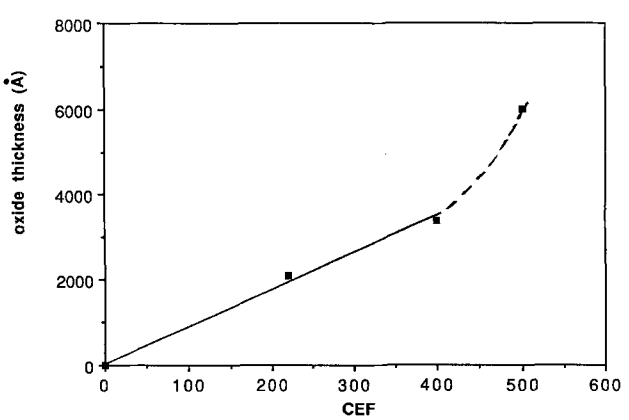

Fig. 7. Oxide film dry thickness (from SEM analysis) vs. CEF; s = 100 mV/s.

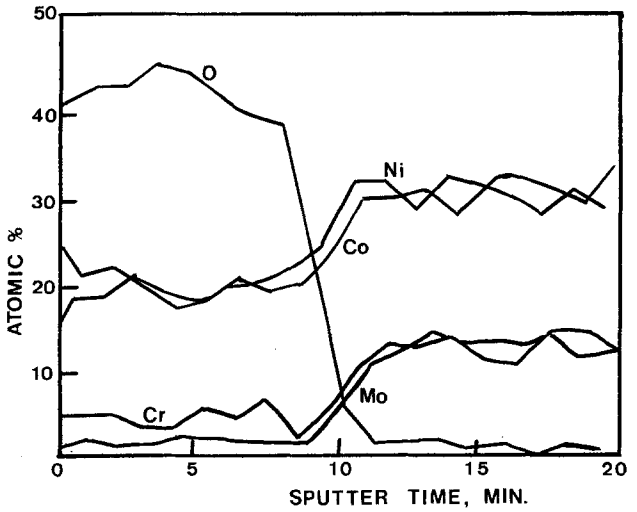

Fig. 8. AES depth profile of electrochemically formed oxide film at Ni-Co amorphous alloy (conditions as in Fig. 3).

retained throughout the film, and is not lost through a dissolution process. XPS data indicate that both Co and Ni are oxidized, while Cr and Mo are also present as oxides, but at a lower concentration than in the original alloy. The reactions occurring in peaks A_2/C_2 can be represented by the following

$$\text{Ni(II)Co(III)oxide} + x\text{OH}^- \rightleftharpoons \text{Ni(III)Co(IV)oxide} + 2e^- \quad [1]$$

If $x > 2$ (36, 37, 62), Na^+ ions must also be involved in the reaction in these solutions. The Co(III) to (IV) transition is suggested in Eq. [1] on the basis of CV peak assignments made for polycrystalline Co electrodes (42, 49, 51).

One possible explanation for the predominance of Ni electrochemistry is that when the potential is negative of the Ni(II)/Ni(III) redox potential of *ca.* 1.3 V, the oxide film, containing at least 50% Ni sites, may be electronically nonconductive. This is consistent with the known poor electronic conductivity of $Ni(OH)_2$ films (63). Therefore, electrons can be transferred to the underlying metal only when Ni(III) sites are generated, and the electronic conductivity of the film increases, thus allowing the oxidation of all the remaining Ni and Co sites within the oxide film. However, this still does not explain why a mixture of Ni and Co electrochemistry is not seen at potentials greater than *ca.* 1.3 V.

It is also possible to interpret the absence of Co electrochemistry in terms of a model in which hydrous oxide films are considered as analogs of particular electroactive polymer films. In the case of redox polymers such as poly 4-vinyl-4′-methyl 2,2′-bipyridine, containing two different redox active metals, *e.g.*, Ru and Fe (64), film oxidation, which is believed to take place by site-to-site electron hopping, cannot occur until the redox potential of both species is exceeded, and only then can both metal components be oxidized, usually in a single step. This is because, in order for electrons to transfer into the film, available states which are stable in a reduced form must be present. By analogy, it is feasible that Co(II) or (III) sites cannot be oxidized until the Ni(II) sites can be readily oxidized to Ni(III), *i.e.*, at potentials greater than *ca.* 1.3 V. Under these conditions, the A_2 peak would reflect the direct oxidation of Ni(II) sites to Ni(III) and the concurrent mediated oxidation of the Co sites within the film.

Conditions influencing oxide growth rate.—Most oxide films were formed by continuous sweeping at 100 mV/s between the potential limits of −0.4 and 1.55 V *vs.* RHE. Under these conditions, particularly in the first few hours, a constant rate of oxide growth was routinely achieved (Fig. 9), indicative of the build-up of a homogeneous film material having essentially constant properties with increasing thickness, and of the absence of changes in the rate-determining step of the oxidation/reduction processes. As the oxide film thickens after longer times of growth, a diminished rate of growth was seen, due both to the development of diffusion-controlled reaction rates and the increasing ohmic resistance of the film. The effect of the upper potential limit, E_+, on the oxide growth rate was studied by measuring the charge in peak C_2 after each scan of potential. The increase in charge density per cycle is shown in Fig. 10 as a function of E_+, for a growth sweep rate of 100 mV/s. Similarly to hydrous oxide growth at Ir electrodes (41), the growth rate increases linearly with E_+, up to *ca.* 1.7 V.

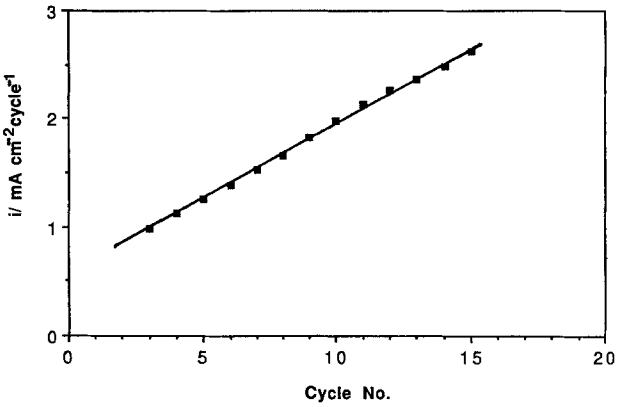

Fig. 9. Initial growth rate of oxide films, as determined from cathodic peak current density. $E_- = -0.4$ V, $E_+ = 1.6$ V, $s = 100$ mV/s.

In the case of Ir electrodes, it has been suggested that an increase in E_+ during growth leads to a more complete conversion of the surface of an underlying inner compact oxide film to a hydrous oxide film, with a maximum of one monolayer of new oxide film being formed per growth cycle (41). It is interesting that the highest growth rate per cycle, obtained with the most positive E_+ shown in Fig. 10, is *ca.* 0.15 mC/cm², which is similar to what would be expected when one monolayer of a typical oxide film undergoes a one-electron reaction, *e.g.*, Ni(III) to Ni(II), in peak C_2. Even after long times at potentials in the OER region, the rate of oxide growth per cycle does not exceed the charge density given above at these amorphous Ni/Co electrodes.

The influence of E_- on the oxide growth rate is illustrated in Fig. 11. The quantity of oxide growth per cycle increases when E_- is extended negatively of 0 V *vs.* RHE, leading to an apparent maximum of *ca.* 0.12 mC/cm². The effect of the lower limit is also similar to the case at Ir (41) and Ni (36, 37) electrodes. With Ir oxide electrodes (41), it was suggested that potentials negative of a critical E_- are required in order to release the newly formed layer of hydrous oxide (formed in the previous excursion to E_+) from the metal surface into the growing hydrous oxide layer lying above.

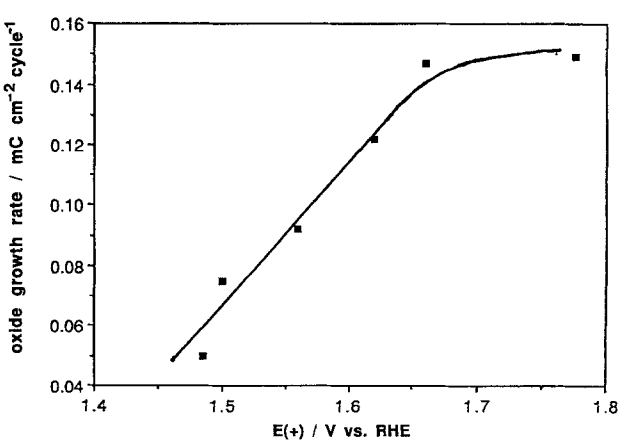

Fig. 10. Effect of E_+ on oxide growth rate in 1M NaOH (determined from peak C_2). $E_- = -0.4$ V, $s = 100$ mV/s.

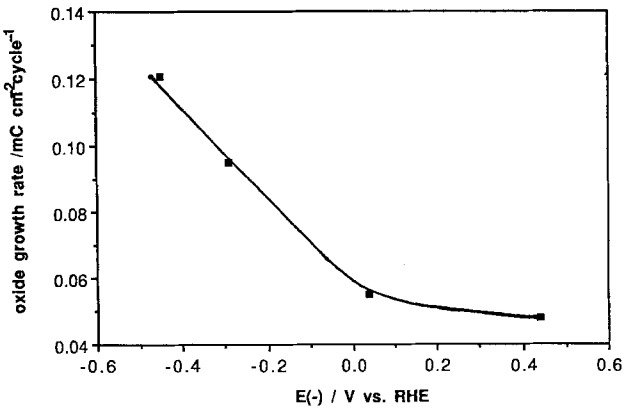

Fig. 11. Effect of E_- on oxide growth rate (from peak C_2). E_+ = 1.6 V; s = 100 mV/s.

It is of interest that the oxide film on this glassy alloy electrode continues to grow, although at a low rate, even when E_- is as positive as 1.0 V. This is very different from the case of polycrystalline Ni electrodes, where E_- must be more negative than *ca.* −0.25 V for oxide growth to occur (37), while at Ir (41), this critical E_- value is *ca.* 0.2 V. On Co electrodes, hydrous oxide film growth can occur when E_- is <0.5 V, although the optimum value is *ca.* 0 V (47).

Another relevant variable is the growth sweep rate. Contrary to the case of Ir electrodes (41), where the optimum sweep rate is *ca.* 1-2 V/s, a maximum oxide growth rate per cycle of *ca.* 0.15 mC/cm^2 (Fig. 12) is achieved at these Ni-Co alloys at very slow sweep rates, *i.e.*, 5-10 mV/s. Clearly, the more time available in each cycle, the more oxide can be formed. Obviously, for practical reasons, higher sweep rates should be used to achieve a higher oxide growth rate per unit time.

A simple test of the importance of time involved the use of a trapezoidal waveform, with an 8 s wait at various E_+ values and a growth sweep rate of 100 mV/s. The oxide growth per cycle was *ca.* 20% higher than with the use of the typical triangular program, and a maximum oxide growth per cycle of *ca.* 0.18 mC/cm^2 was consistently obtained. The fact that the maximum growth rate per cycle is similar to the charge density observed in the first few cycles of potential of an as-received electrode supports the assumption that a value of *ca.* 0.15 to 0.20 mC/cm^2 represents one monolayer of oxide film at these electrodes.

Mechanism of hydrous oxide growth.—An important observation in this work has been the maximum oxide growth rate of *ca.* 0.15 to 0.20 mC/cm^2 at the amorphous Ni-Co alloy. This is similar to the expected charge density for a one-electron transfer reaction within a single layer of hydrous oxide film (41). Also, the requirement for cycling between positive and negative potentials to achieve oxide growth is similar to previous observations during hydrous oxide growth at metals such as Ir (41). Therefore, it is reasonable to suggest that a similar type of oxide film and a similar growth mechanism pertains in these two cases.

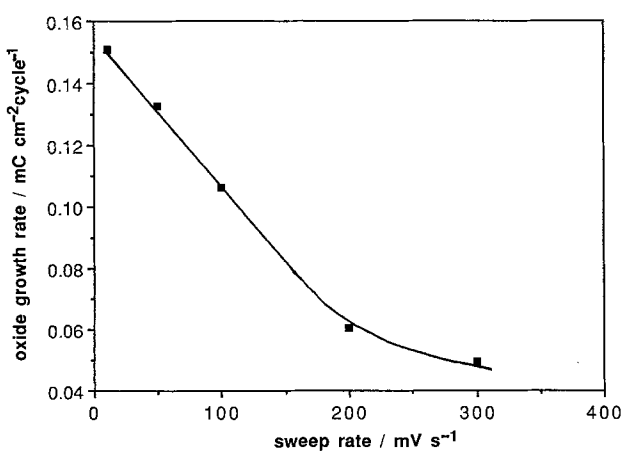

Fig. 12. Effect of potential sweep rate on oxide growth rate. E_+ = 1.65 V; E_- = −0.1 V.

Based on this analogy, it is suggested that in each excursion to E_+, the underlying metal surface or the surface of a thin, compact oxide film, attached to the metal, can be oxidized to a higher state, which can readily be hydrated, perhaps due to a unique structure/porosity induced by concurrent oxygen evolution and/or some metal dissolution (41). It is suggested that this newly formed hydrous surface oxide remains attached to the underlying electrode surface until the reaction in peak C_2 is complete and the potential is extended more negatively. The monolayer of newly formed oxide is then released from the metal surface to the bulk of the oxide film, so that in the next positive sweep, the alloy surface beneath the growing hydrous oxide film is available again for the formation of up to one monolayer of new hydrous oxide.

The rapid rate of hydrous oxide growth on the amorphous Ni-Co alloy, as compared to the behavior of polycrystalline Ni electrodes, as well as the presence of Co within the oxide film and yet the absence of its electrochemical signature, are indicators of some new properties of this oxide film. It is possible that the oxide which is formed is a spinel-like material, and that the observed behavior reflects that of an electrodeposited material of this kind. It is also possible that the amorphous state of the substrate has produced a new type of amorphous Ni-Co oxide film, having somewhat different properties than similar oxides formed by high-temperature methods (65), on conventional co-precipitated Ni-Co electrodes (66) or Co-Ni alloys (53).

It may also be relevant that at a fresh polycrystalline Ni electrode, a comparatively thick (*ca.* 10 monolayers) $Ni(OH)_2$ film is formed in the potential range from peak A_0 to A_2 in the first sweep of potential in alkaline solutions (Fig. 2, upper left). This film is known to be a poor electronic conductor, and is believed to thicken by a field-assisted ionic migration mechanism (67). It is reasonable to suggest that the oxidation of *ca.* 10 monolayers of a compact, non-conductive Ni(II) oxide in peak A_2 is likely to produce a relatively compact, non-porous Ni(III) oxide film, which could be difficult to convert to a porous, hydrated material. Possibly for this reason, hydrous oxide growth is slow at Ni electrodes, and requires rather extreme electrochemical conditions, as compared to the case at these amorphous Ni-Co alloys.

In the present work, the enriched state of Cr (and B) at the original amorphous alloy surface has been shown to lead to the formation of only a very thin Ni(II)-Co(II) film in the first sweep, such that when the potential for the Ni(II) to Ni(III) conversion process is reached, this occurs readily and the film can be easily hydrated. Therefore, one of the key reasons for the rapid growth rate of hydrous oxides at the Ni-Co amorphous alloy may be the inhibition of the formation of a significant amount of the compact Ni(II) oxide film, perhaps by the presence of Cr, and other elements, at the original alloy surface. Once these are removed by dissolution at *ca.* 1.0 V, the potential may be high enough to generate a hydrous oxide film directly. The presence of Co in the alloy, at which hydrous oxide growth is known to occur by a monolayer-by-monolayer mechanism, may also be an important influence in the nature and rate of the growth of hydrous oxides at these Ni-Co amorphous alloys.

Summary

The surface of a Ni-Co amorphous alloy has been found to be enriched in Cr (and possibly B), as seen by AES profiles and the preferential electrochemical dissolution of these elements in the first anodic cycle in 1*M* NaOH solutions. Following this, continuous potential cycling leads to the build-up of an oxide film, initially linearly with cycling time, but at a decreasing rate as the film thickens. The film thickness, as determined by SEM, can reach 1 μm. It has the classical mud-cracked structure of hydrous oxide films formed at metals such as Ir and Rh, and displays a similar thickness/charge density relationship. The optimum po-

tential limits for oxide growth have been found to be *ca.* 1.7 V and −0.4 V, with the maximum oxide growth rate occurring at slow sweep rates or by holding the potential for periods of time at both the upper and lower limits.

The electrochemical response appears to be quite similar to that observed with polycrystalline Ni electrodes; no distinct signature is observed for Co, although Co remains in the oxide film, as seen by AES analysis. It is suggested that the Co sites may react in a mediated fashion only when the Ni(II)/(III) potential is exceeded, similar to the case of a number of polymer-modified electrodes containing more than one transition metal. The mechanism of hydrous oxide growth on these alloys is suggested to be similar to that of Ir electrodes, *i.e.*, involving the transformation of the underlying metal surface to up to a monolayer of hydrated metal oxides at positive potentials, and its release into the bulk of the oxide film at negative potentials. The ease of oxide growth at these electrodes compared to polycrystalline Ni, for example, may be related to the formation of only *ca.* one monolayer of poorly conducting Ni/Co(II) oxide in the potential range between the HER and that of the principal reaction, perhaps facilitating its conversion to the hydrous oxide at higher potentials.

Acknowledgments

We gratefully acknowledge financial support from the Natural Sciences and Engineering Research Council, and also thank Dan Tilleman for assistance with the SEM analyses of our specimens. We also express our gratitude to Allied-Signal Corporation for providing the glassy alloy samples, to Dr. J. Brown, at CANMET/EMR, and to Dr. D. Lloyd, at Alcan International Limited, for the XPS and AES analyses.

Manuscript submitted Feb. 15, 1991; revised manuscript received June 20, 1991. This was Paper 215 presented at the Honolulu, HI, Meeting of the Society, Oct. 18-23, 1987.

REFERENCES

1. P. Chaudhari, B. C. Giessen, and D. Turnbull, *Sci. Am.*, **242,** 98 (1980).
2. J. J. Gilman, *Science,* **208,** 856 (1980).
3. T. Masumoto, in Proc. 4th Int. Conf. Rapidly Quenched Metals, I, p. 5 (1982).
4. H. Fujimori, *ibid.*, II, p. 1101 (1982).
5. C. D. Graham and T. Egami, *Ann. Rev. Mater. Sci.*, **8,** 843 (1978).
6. D. L. Cocke and C. Yoon, in Proc. 5th Int. Conf. Rapidly Quenched Metals, I, p. 27 (1986).
7. K. Hashimoto, *ibid.*, II, p. 1449 (1986).
8. Y. Waseda and J. M. Toguri, *Metall. Soc. Can. Inst. Min. Metall.*, **16,** 133 (1977).
9. "Amorphous Metallic Alloys," F. E. Luborsky, Editor, Butterworths, London (1983).
10. H. Warlimont, in Proc. 6th Int. Conf. Rapidly Quenched Metals, III, R. W. Cochrane and J. O. Strom-Olsen, Editors, p. 1 (1988).
11. M. Naka, K. Hashimoto, and T. Masumoto, *J. Jpn. Inst. Metal,* **38,** 835 (1974).
12. T. Masumoto and K. Hashimoto, *Ann. Rev. Mater. Sci.*, **8,** 215 (1978).
13. R. D. Diegle, *J. Non-Cryst. Solids,* **61** and **62,** 601 (1984).
14. Y. Waseda and K. Aust, *J. Mater. Sci.*, **1619,** 2337 (1981).
15. M. D. Archer, C. C. Corke, and B. H. Herji, *Electrochim. Acta,* **32,** 13 (1985).
16. K. Cho, C-H. Hwang, C-S. Park, and Y-J. Ryeom, Proc. 4th Int. Conf. Rapidly Quenched Metals, 1467 (1982).
17. K. Cho, C-H. Hwang, Y-J. Ryeom, and C-S. Park, *ibid.*, 1479 (1981).
18. R. B. Diegle, N. R. Sorensen, T. Tsuru, and R. M. Latanision, in "Treatisé on Materials Science and Technology," **23,** J. C. Scully, Editor, p. 59, Academic Press, London (1983).
19. N. C. Grant and M. D. Archer, *This Journal,* **131,** 997 (1984).
20. *Ibid.*, **131,** 1004 (1984).
21. M. Naka, K. Hashimoto, T. Masumoto, and I. Okamoto, in Proc. 4th Int. Conf. Rapidly Quenched Metals, I, 1431 (1982).
22. G. Kreysa and B. Hakansson, *J. Electroanal. Chem.*, **201,** 61 (1986).
23. M. Enyo, T. Machida, and K. Yoshida, in Corrosion, Electrochemistry, and Catalysis of Metallic Glasses, (PV 88-1) R. B. Diegle and K. Hashimoto, Editors, pp. 380-389, The Electrochemical Society Softbound Proceedings Series, Pennington, NJ (1988).
24. J-Y. Huot and L. Brossard, *Int. J. Hydrogen Energy,* **12,** 519 (1987).
25. M. Enyo, T. Yamazaki, K. Kai, and K. Suzuki, *Electrochim. Acta,* **28,** 1573 (1983).
26. K. Machida, T. Yamazaki, K. Kai, and K. Suzuki, *Bull. Chem. Soc. Jpn.*, **56,** 3393 (1983).
27. H. Alemu and K. Juttner, *Electrochim. Acta,* **33,** 1101 (1988).
28. A. Yokoyama, H. Komiyama, H. Inoue, T. Masumoto, and H. M. Kimura, *Chem. Lett.*, 195 (1983).
29. M. Shibata and T. Masumoto, in "Preparation of Catalysts," IV, B. Delmon, P. Grange, P. A. Jacobs, and G. Poncelet, Editors, Elsevier Science Publishers, B. V. Amsterdam, 353 (1987).
30. J. L. Weininger and M. W. Breiter, *This Journal,* **110,** 484 (1963).
31. *Ibid.*, **111,** 707 (1964).
32. H. Bode, K. Dehmelt, and J. Witte, *Electrochim. Acta,* **11,** 1079 (1966).
33. G. W. D. Briggs and M. Fleischmann, *Trans. Faraday Soc.*, **62,** 3217 (1966).
34. C. M. MacArthur, *This Journal,* **117,** 422 (1970).
35. L. D. Burke and D. P. Whelan, *J. Electroanal. Chem.*, **109,** 385 (1980).
36. L. D. Burke and T. A. M. Twomey, *ibid.*, **167,** 285 (1984).
37. *Ibid.*, **134,** 353 (1982).
38. R. S. S. Guzman, J. R. Vilche, and A. J. Arvia, *Corros. Sci.*, **18,** 765 (1978).
39. W. Visscher and E. Barendrecht, *Surf. Sci.*, **135,** 436 (1983).
40. D. N. Buckley and L. D. Burke, *J. Chem. Soc. Faraday Trans. 1,* **71,** 1447 (1975).
41. P. G. Pickup and V. I. Birss, *Electroanal. Chem.*, **220,** 83 (1987).
42. *Ibid.*, **240,** 171 (1988).
43. *Ibid.*, 185.
44. P. G. Pickup and V. I. Birss, *This Journal,* **135,** 127 (1988).
45. D. N. Burke and E. J. M. O'Sullivan, *J. Electroanal. Chem.*, **93,** 11 (1978).
46. L. D. Burke, T. A. M. Twomey, and D. P. Whelan, *Electroanal. Chem.*, **107,** 201 (1980).
47. L. D. Burke, M. E. Lyons, and O. J. Murphy, *ibid.*, **132,** 247 (1982).
48. L. D. Burke and O. J. Murphy, *ibid.*, **109,** 373, 379 (1980).
49. W. K. Behl and J. E. Toni, *ibid.*, **31,** 63 (1971).
50. H. G. Meier, J. R. Vilche, and A. J. Arvia, *ibid.*, **134,** 251 (1982).
51. *Ibid.*, **138,** 367 (1982).
52. P. Rasiyah and A. C. C. Tseung, *This Journal,* **129,** 1724 (1982).
53. J. Haenen, W. Visscher, and E. Barendrecht, *Electrochim. Acta,* **31,** 1541 (1986).
54. R.-N. Singh, M. Hamdani, J.-F. Koenug, G. Poillerat, J. L. Gautier, and P. Chartier, *J. Appl. Electrochem.*, **20,** 442 (1990).
55. K. Lian, M. Sc. Thesis, University of Calgary (1988).
56. D. Majumdar, R. G. Spahn, and J. S. Gau, *This Journal,* **134,** 1825 (1987).
57. V. Birss, R. Myers, H. Angerstein-Kozlowska, and B. E. Conway, *ibid.*, **131,** 1502 (1984).
58. M. Farebrother, M. Goledzinowski, G. Thomas, and V. I. Birss, *J. Electroanal. Chem.*, **297,** 409 (1991).
59. A. C. Chialvo, W. E. Triaca, and A. J. Arvia, *ibid.*, **146,** 93 (1983).
60. V. Birss, Unpublished results.
61. K. Lian and V. I. Birss, *This Journal,* **138,** 2885 (1991).
62. L. D. Burke and T. A. M. Twomey, *Electroanal. Chem.*, **162,** 101 (1984).
63. J. P. Hoare, "The Electrochemistry of Oxygen," Interscience, New York (1968).
64. P. G. Pickup, C. R. Leidner, P. Denisen, and R. W. Murray, *Electroanal. Chem.*, **104,** 39 (1984).
65. G. C. Wood and B. Chattopadhyay, *Corros. Sci.*, **10,** 471 (1970).
66. D. F. Pickett and J. T. Maloy, *This Journal,* **125,** 1026 (1978).
67. A. Damjanovic and W. Visscher, Unpublished results.